

Experimental Acoustic Modal Analysis of an Automotive Cabin

Giampiero Accardo, Bart Peeters, Fabio Bianciardi, and Karl Janssens,

Siemens Industry Software, Leuven, Belgium

Mahmoud EI-kafafy, Vrije Universiteit Brussels, Brussels, Belgium

Daniele Brandolisio, Katholieke Universiteit, Leuven, Belgium

Milena Martarelli, Università degli Studi eCampus, Novedrate, Italy

The interior sound perceived in an automobile cabin is a very important attribute in vehicle engineering. Therefore, an ever-increasing interest exists to predict the interior acoustic behavior by means of accurate simulation models both to improve the vehicle NVH performance and to reduce the development cycle of a new vehicle. Nevertheless, the current level of accuracy of such models is not sufficient to replace the design prototype phase with an all-digital phase. Experimental methods in which an acoustic characterization is performed play an important role in understanding the modeling challenges, improving the overall modeling know-how and providing a detailed comprehension of the physical behavior. Besides these longer-term objectives, experimental acoustic methods are also instrumental as part of a vehicle development program and to refine the design; for example, troubleshooting booming noise. By means of a case study on a fully trimmed sedan car, this article discusses acoustic modal analysis equipment requirements and testing procedures. Due to specific challenges, such as high modal damping ratios and the need to use a large number of sound sources spread around the cabin to get a sufficient excitation of the modes, modal parameter estimation is often not a trivial task. The modal parameters (resonance frequencies, damping ratios, mode shapes, and modal participation factors) will be estimated from the measured frequency response functions by the new ML-MM method, a multiple-input, multiple-output frequency-domain maximum likelihood estimator based on a modal model formulation.

The interior sound quality of a car is an important decision factor for customers when purchasing a new car. Therefore, this attribute is carefully considered and controlled in the design process. To improve the interior noise performance, CAE predictions have gained importance, especially in the early development stage when it is still possible to make changes without negatively affecting vehicle development time.

An acoustic finite-element (FE) model of a vehicle cabin is an important component of a structural-acoustic numerical model for interior noise simulation. Such a model can be used to fine-tune the structural and acoustic design of the cabin to achieve specific NVH objectives. It can also be used as a diagnostic tool to identify potential noise sources and also to evaluate the effectiveness of proposed design modifications. It is obvious that the effectiveness of this approach greatly depends on the accuracy of the predictions made using such a model. To understand the modeling challenges and improve the overall acoustic modeling know-how, experimental acoustic characterization of the cabin plays a crucial role.

When performing an interior acoustic study, it is important to relate the acoustic responses to the intrinsic system behavior of the cabin. This can be done by means of acoustic modal analysis; that is, modal parameter estimation methods decompose the system behavior into a set of individual resonance phenomena, each characterized by a resonance frequency, damping ratio, participation factor and mode shape. The experimental dataset to derive this model consists of a set of frequency response functions (FRFs) between a set of reference (acoustic source input) degrees of freedom and all response (measured sound pressure) degrees of freedom.

Based on a paper presented at IMAC-XXXIII, the 33rd International Modal Analysis Conference, Orlando, FL, February 2015.

Specific acoustic modal analysis challenges are the high modal damping ratios resulting in highly overlapping modes and the need to use a large number of references distributed around the cabin to get a sufficiently homogenous sound field.^{1,2} These challenges call for a specific modal parameter estimation method that is able to cope with FRF matrices with many columns (four or more) related to the use of many input locations.

This article focuses on the experimental modal analysis of an automobile cabin. Here modal parameters will first be estimated by the well-known LMS Polymax method,³ and then by the ML-MM estimator, where the error between the modal model equation and the measured FRF data is minimized in a maximum likelihood sense.^{4,5}

This article is organized as follows: We review the theory of acoustic modal analysis. Using a discretized formulation, one can see that an analogy exists between acoustical and mechanical systems. Thanks to this equivalence, the classical approach can be used also in the acoustic modal analysis case, if one uses the correct measurement quantities. We then discuss a newly developed sound source that is particularly suited for acoustic modal analysis testing. We then present a case study on a fully trimmed car. Test preparation, set-up and measurements are described in detail. To have an idea of the expected acoustic modes, a numerical model was created and used for a preliminary analysis. This model was instrumental to study the proper distribution of sources and to prepare the geometry of the microphones capturing pressure response inside the automobile cabin. Measurement points, sources and their respective location are presented. After the validation of the measurement chain, we discuss modal parameter estimation. Two different methods are used for this purpose: LMS Polymax and the new ML-MM method that iterates further on the Polymax initial values.

Theory of Acoustic Modal Analysis

In this section, only a brief theoretical overview is given. Many references can be consulted for further details about the model formulations describing the dynamic behavior of vibro-acoustic systems.^{6,7}

Here boundaries of the enclosure will be modeled as rigid walls, so the dynamic behavior of a pure acoustic system is described. By considering a three-dimensional closed acoustic system with rigid or finite impedance but non-vibrating boundaries, the governing equation of the system, excited by a point monopole of volume velocity at \mathbf{r}_0 can be written as:⁶

$$\nabla^2 p(\mathbf{r}, t) - \frac{1}{c^2} \ddot{p}(\mathbf{r}, t) = -\rho q \delta(\mathbf{r} - \mathbf{r}_0) \quad (1)$$

where p is the sound pressure, which is a function of space \mathbf{r} and time t ; c is the speed of sound; ρ is the density of the medium; and q is the volume velocity. The boundary condition over the rigid surface S is:

$$\frac{\partial p}{\partial \mathbf{n}} = 0 \quad \text{over } S \quad (2)$$

where \mathbf{n} is the internal unit normal to S .

The discretization of the continuous acoustic wave equation is based on the finite element formulation. The acoustic domain of volume V is represented by an assemblage of acoustic finite

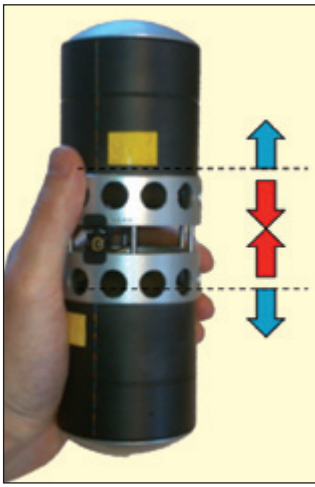


Figure 1. LMS Qsources low-frequency monopole sound source (Q-MED).

elements. The pressure distribution within an element is interpolated in terms of the nodal pressures by using shape functions. Variational formulation based on the differential equation (1), boundary condition (2) and FE discretization gives the \mathbf{M}^f , \mathbf{C}^f and \mathbf{K}^f matrices. To preserve the analogy with a structural finite-element model, the matrix \mathbf{M}^f is called the acoustic mass matrix, although it represents a compressibility matrix relating the pressure to a displacement. The matrix \mathbf{C}^f is the acoustic damping matrix, induced by the impedance boundary condition. The matrix \mathbf{K}^f is called the acoustic stiffness matrix,

although it represents an inverse mass or mobility matrix, relating the pressure to an acceleration. Assuming now that a number of point monopoles of known volume velocity are placed in the cabin and the sound pressure across the volume is sampled at an appropriate number of points, it can be shown that the continuous-wave equation can then be substituted by its discrete equivalent:

$$\mathbf{M}^f \ddot{\mathbf{p}} + \mathbf{C}^f \dot{\mathbf{p}} + \mathbf{K}^f \mathbf{p} = -\rho \dot{\mathbf{q}} \quad (3)$$

Note that in the present formulation, one-way coupling between the structure and the interior acoustic domain is assumed. This approximation is acceptable for the cases where the acoustic loading on the structures is negligible, like in automotive NVH applications, where air is the medium.⁸ The discrete governing equation above is equivalent to the discrete mechanical equations of motions, with \mathbf{M}^f , \mathbf{C}^f , \mathbf{K}^f in the role of mass, damping, and stiffness matrices; \mathbf{p} in the role of displacement; and $\dot{\mathbf{q}}$ in the role of force.

Assuming zero initial conditions, the Laplace-transform of the previous equation reads:

$$\left[s^2 \mathbf{M}^f + s \mathbf{C}^f + \mathbf{K}^f \right] \cdot \mathbf{p}(s) = -\rho s \mathbf{q}(s) \quad (4)$$

As usual in structural dynamics, the inverse of the matrix term can be substituted by the frequency response function $\mathbf{H}(s)$:

$$\mathbf{p}(s) = -\rho s \mathbf{H}(s) \cdot \mathbf{q}(s) \quad (5)$$

One can prove that the FRF-matrix can be expressed as a partial fraction expansion of modal parameters:⁹

$$\mathbf{H}(s) = \sum_{r=1}^{N_m} \frac{Q_r \phi_r \phi_r^T}{s - \lambda_r} + \frac{Q_r^* \phi_r^* \phi_r^{*T}}{s - \lambda_r^*} \quad (6)$$

where N_m is the number of modes, ϕ_r the r -th modal vector, Q_r the modal scaling factor for the r -th mode, and λ_r the system pole for the r -th mode. Substituting s with $j\omega$ and using Eq. 5, it is obvious that the modal parameters of the system can be gained from the FRF measurements where the sound pressures across the volume are referenced to the volume velocities of the sources. The Equations 4 through 6 are in complete analogy with those being used in structural dynamics, so we conclude that the classical modal parameter estimation approach can be also followed in the acoustic modal analysis case.

An interesting expansion toward experimental coupled vibro-acoustic modal analysis is provided in Reference 10.

New Sound Source

Sources used for an acoustic modal analysis have been originally developed to enable transfer-path analysis (TPA) and airborne source quantification (ASQ). These sources do have either no effect on the acoustic field (LMS Qsources Miniature Source or Q-IND) or have dimensions that are similar to a human torso and produce very high low-frequency noise levels (LMS Qsources Low Mid Frequency Source or Q-LMF). The latter will result in high-quality acoustic and vibro-acoustic FRFs with the assumption that

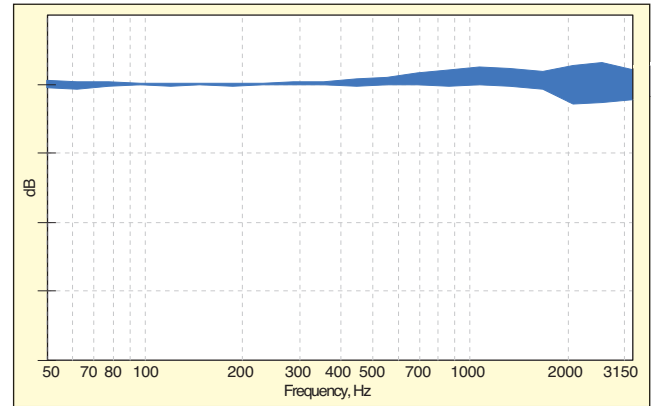


Figure 2. Directivity plot at 1 meter in semi anechoic conditions (Y tick divisions = 10 dB).

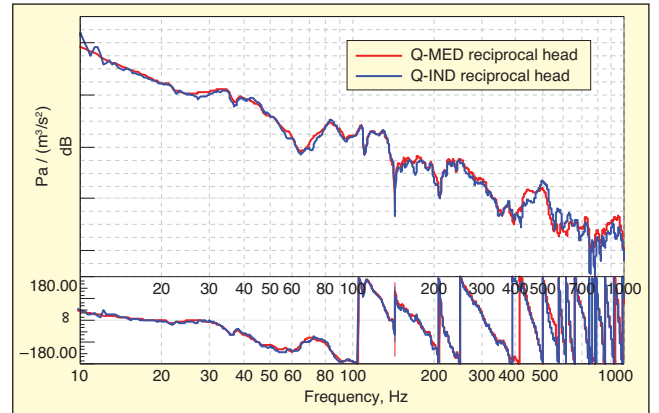


Figure 3. In-vehicle acoustic FRF measured with two different sound sources (Y tick divisions = 20 dB).

occupants are present in the vehicle. This is an important feature for transfer-path analysis of interior noise. The miniature source has, due to its miniature size, no body diffraction and emits the noise as a monopole source up to several kHz. In high-end vehicles where local damping is also very high, the noise level, necessary for acoustic FRFs in the cabin is at its limits. So the need exists for a dedicated source that is compact, omnidirectional and capable of generating high noise levels in the low-frequency range.

The LMS Qsources Low-Frequency Monopole Sound Source (Q-MED) is a unique monopole sound source (Figure 1) that has been developed to acquire acoustic and vibro-acoustic FRFs accurately without disturbing the acoustic behaviour of the passenger compartment. The main design drivers were high noise levels at low frequencies, omnidirectional behavior and real-time sound source strength measurements. This has been accomplished by using two high-performance magnetic drivers with a patent-pending voice coil stroke assembled within a rigid body.

The FRF database for modal analysis should be as accurate as possible. One of the elements is an omnidirectional sound source. This allows an accurate real-time, sound-source strength measurement. Figure 2 clearly shows that the emitted sound pressure does not vary more than 1.5 dB at 630 Hz. A comparison of acoustic FRFs measured in the passenger compartment of a compact vehicle with an LMS Qsources Miniature Source is shown in Figure 3. The FRFs are visibly identical, although the size of both sources varies significantly. The LMS Qsources Miniature Source measures only 71 mm long \times 22 mm in diameter, while the new LMS Qsources Low Frequency Monopole Sound Source measures 200 mm long \times 70 mm in diameter. The comparison shows that there are no relevant directional effects that deteriorate the FRFs measured with the larger source.

The noise level of the acoustic source should make FRF measurements possible between all measurement points in the cabin even when the trunk is being included in the analysis. Figure 4 shows a typical FRF where the acoustic source is placed in the trunk and a response has been measured in the front-row foot area. The

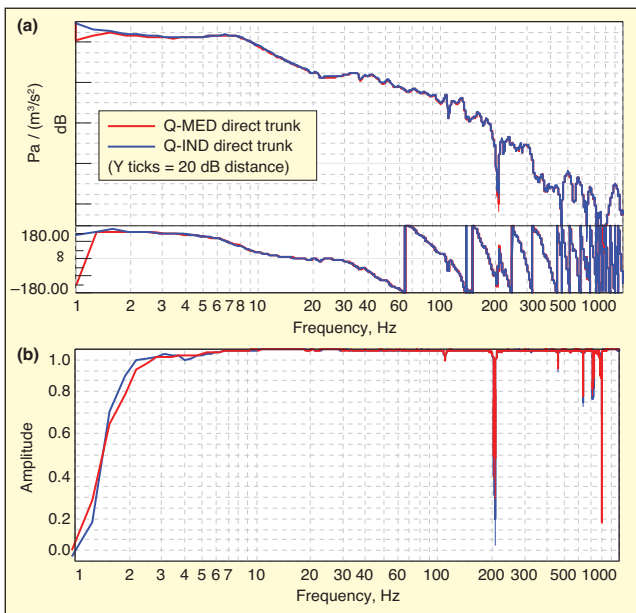


Figure 4. Repeatability of FRF measurements.

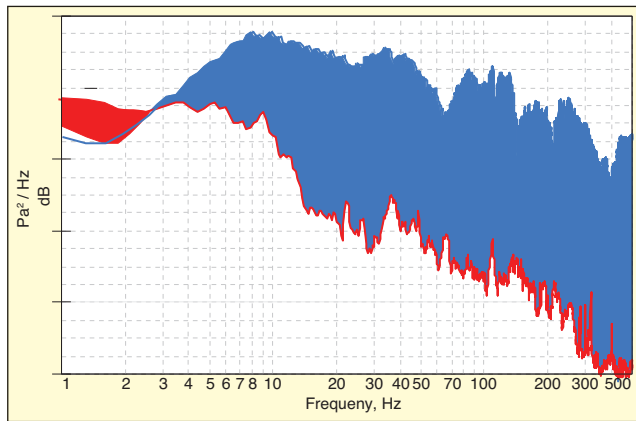


Figure 5. Noise level versus background noise (Y ticks = 20 dB distance).

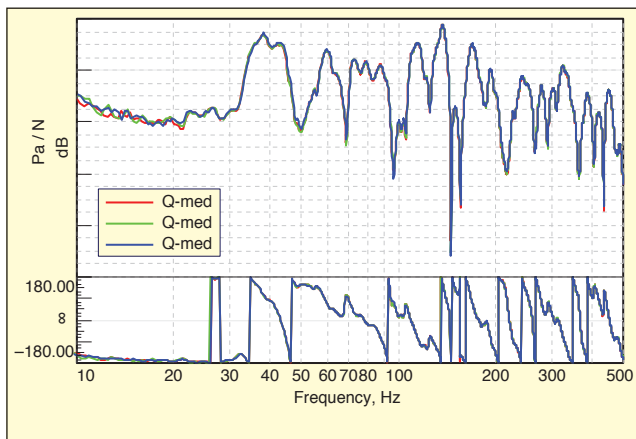


Figure 6. Repeatability of vibro-acoustic FRF measurements.

coherence is shown in Plot b for two measurements. The coherence between input and output are close to 100% from 10 Hz on. Repetitive measurements also result in identical FRFs. At higher frequencies some coherence drops are caused by anti-resonances in the measured FRF.

The measurements have been carried out in semi-anechoic test laboratories at the LMS Engineering Services facilities in Belgium. Figure 5 shows a comparison between a microphone response in the trunk when the source is active and when the source is switched off. Above 10 Hz, the artificial noise generation results in a response that is up to 50 dB higher, guaranteeing that FRFs can

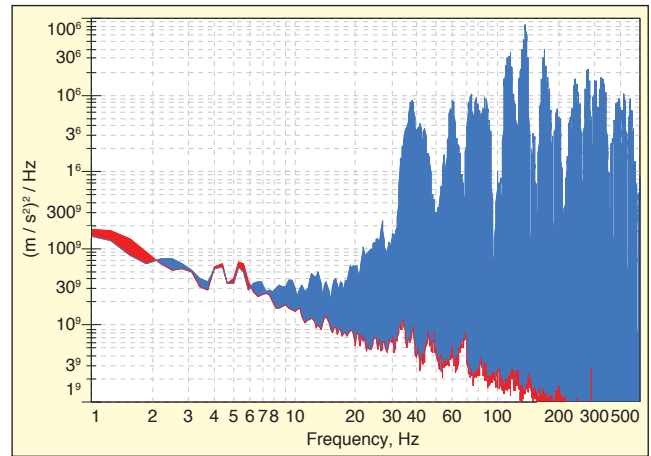


Figure 7. Acceleration PSD and background noise.

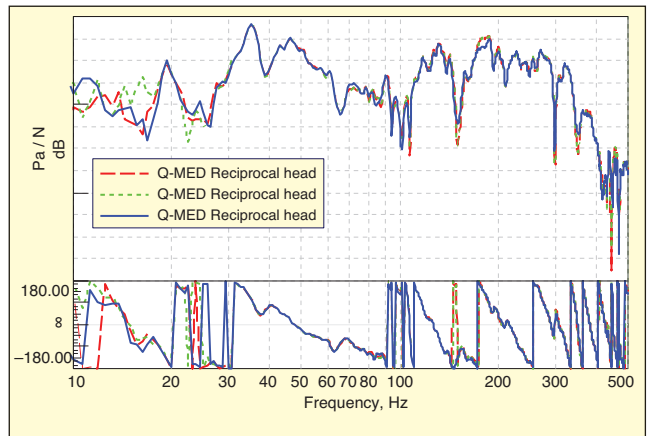


Figure 8. Vibro-acoustic FRF (Y tick divisions = 20 dB).

be measured in workshops where background levels are typically somewhat higher.

Next to acoustic-acoustic FRFs, the Q-MED enables the acquisition of vibro-acoustic FRFs. These FRFs include information about the interaction between the acoustic cabin and surrounding panels at the boundary, which can be used to correlate simulation models that include both acoustic and structural elements. Figure 6 shows three consecutive FRF measurements indicating highly repeatable measurements. The structural response due to the source excitation is significantly higher than the accelerometer self-noise above 10 Hz. This is shown in Figure 7.

The Q-MED even allows measuring vibro-acoustic FRFs to potential structure-borne noise source interfaces such as powertrain mounts. These data also contain the sensitive frequencies because of the acoustic modes. Advanced analysis, such as TPA, is now possible to understand structure-borne noise generation. Figure 8 contains three consecutive vibro-acoustic FRFs, where the source has been positioned at the driver ear location and the structural acceleration response has been measured at one engine mount.

Acoustic Modal Analysis Test Campaign

Before describing the test campaign and the estimation of the acoustic modes of the cavity of a fully trimmed sedan car (Figure 9), a preliminary analysis with a finite-element (FE) model is presented. Such a model will be used as a baseline for the number and shapes of the acoustic modes of the system. The selected car for this case study is the property of Siemens Industry Software and is often used for NVH research. The description of the measurements focus on the experimental set-up, its validation and the following experimental procedure.

Preliminary Analysis. An acoustic FE model (Figure 10) of the interior car cabin with rigid boundaries was created in LMS Virtual.Lab Acoustics to preliminarily know the mode shapes and the number of acoustic modes expected in the frequency range of interest, 0-200 Hz. The internal cabin was modeled with more than



Figure 9. Fully trimmed car used in the case study.



Figure 10. CAE cavity model.

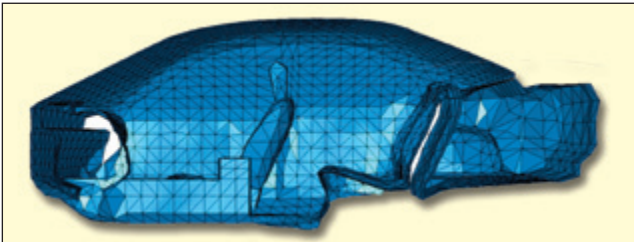


Figure 11. Cavity cross-section.

65000 solid tetrahedral elements and more than 130000 degrees of freedom. As visible in Figures 10 and 11, the model also includes the geometry of the seats and the trunk compartment. Proper physical characteristics of the air are defined for the fluid elements. Under the assumption of rigid boundaries, the real eigensolution analysis shows that there are about 10 uncoupled eigenmodes in the frequency range of interest (see Table 1 and Figure 12).

Note that the model does not take into account any trim materials and any flexible boundary walls, so the eigenmodes from this rough model are not expected to be very close to the real ones. Nevertheless, at this first stage, this model is extremely useful for getting an idea of the number of modes and their shapes. Furthermore, information from the numerical model about the mode shapes are fundamental in order to:

- Know where to properly locate the sound sources to avoid nodal lines.
- Have a preliminary geometry of the measurement points.
- Select meaningful modes and address the dominant acoustic modes in such a coupled system where the FRFs are also influenced by the resonances of the structural system having a much higher modal density than the acoustic one.^{2,11}

Experimental Setup. Multiple acoustic excitation tests were carried out inside the cabin of the sedan shown in Figure 9. Thirty-four microphones located both on a roving array with spacing equal to around 20 cm and near boundary surfaces captured the responses simultaneously. A total of 18 runs were performed to measure the pressure distribution over the entire compartment (both cabin

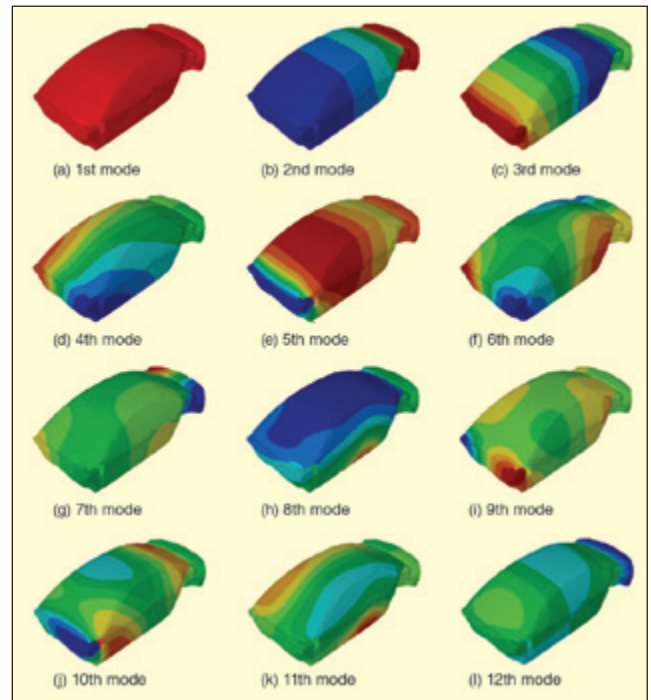


Figure 12. CAE Mode shapes: amplitude and phase.

and trunk). To speed up the measurement process and to reduce the risk of data inconsistencies, more microphones and more acquisition channels could be used. For each run, up to 12 acoustic sources switched on sequentially were used for acoustic excitation. If enough sources were available, they could have also been used simultaneously, provided they were excited by uncorrelated signals, enabling multiple-input FRF estimation. This further sped up the acoustic modal analysis test.

An accurate description of the acoustic modes can be achieved by placing arrays of microphones at as many different locations as possible in the vehicle to increase the observability of the modes and to have more degrees of freedom for the correlation and updating of the FE numerical model.

The pressure responses were measured both at the boundary surface and inside the cabin by positioning the microphones approximately every 20 cm (Figure 13). The mesh of measurement points was preliminarily defined by means of the CAE model. Afterward, the coordinates were updated to reflect the actual test scenario. Sensors were also placed in extreme positions, such as in foot regions, between the windshield and the dashboard, and in the hat shelf region, making a total of 526 measurement points. The same spacing and approach were followed for the trunk as well.

An additional 12 microphones located 2 cm away from the acoustic sources were kept fixed to check the repeatability of the measurements. Additionally, four uniaxial accelerometers were placed on the structure at fixed locations to check repeatability and to analyze vibroacoustic coupling effects.

Table 1. Eigenfrequencies of CAE model with rigid walls.

No.	Frequency, Hz	Mode Shape
1	≈ 0	Rigid Body
2	44.53	I longitudinal
3	85.81	I longitudinal and rigid-body trunk
4	112.42	I lateral
5	128.42	II longitudinal and rigid-body trunk
6	141.06	I longitudinal and I lateral
7	150.20	I longitudinal and I lateral and I lateral trunk
8	155.57	I vertical
9	178.03	II longitudinal and I lateral and I lateral trunk
10	181.97	
11	201.20	I lateral and I vertical and I lateral trunk
12	205.98	III longitudinal



Figure 13. Measurement points. (a) Test model derived from CAE model with markers indicating all microphone locations; (b) Array of microphones inside the cavity; (c) Measurement locations on boundary surface.

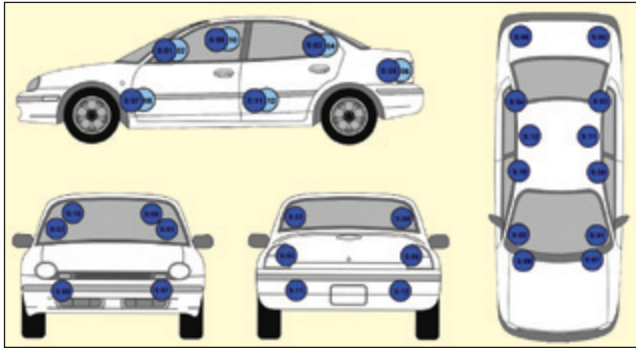


Figure 14. Distribution of source locations in the car cabin.



Figure 15. Detailed view of source locations and used sources.

Calibrated volume acceleration sound sources are necessary to measure acoustic FRFs that are required in acoustic modal analysis. Sound sources have to be omnidirectional and have a negligible size in order not to influence the field, mainly in the higher frequency ranges.¹² As shown numerically (Ref.13) and experimentally (Refs. 1 and 2), an appropriate source distribution over the entire cabin is required to properly excite the acoustic modes.

Too few sources do not allow the right identification of the mode shapes as exciter-location-dependent mode shape distortions are clearly visible. For this reason, a rather large number of sources and source locations were used to excite as many modes as possible. Up to 12 sound sources were set in geometrically symmetric locations, close to the edges, corners and at the maximum amplitude locations to avoid nodal lines and excite close to pressure maxima on the boundaries. Locations of the mentioned excitation points are shown in Figure 14.

Due to its unavailability at the time of the test, the new Q-MED source (described previously) could not be used. Therefore, multiple miniature sources (Q-IND) and two low-mid frequency sources (Q-LMF) were installed in the cabin as shown in Figure 15. The Q-LMF sources have the advantage of providing high noise levels of excitation (extremely high coherence) in low frequency ranges; conversely, they have the disadvantage of having a non-negligible size, as shown in Figure 16. Coster et al.¹⁴ reported that the effect of the source body diffractions and source directivity are negligible up to 100 Hz in free-field condition. As visible in Figure 17, the presence of these sources inside the cabin influences the acoustic field from 80 Hz onward.

So it's noteworthy that the FRFs will be partially affected by the presence of the Q-LMF sources. For this reason, these sources have been kept fixed on the front seats during the whole test campaign in order to not introduce measurement data inconsistencies by varying volume distortions. A numerical simulation taking into account the sources located as in the real scenario (Figure 18), has shown that the eigenfrequencies are slightly shifted in the frequency range of interest. Comparing the eigenfrequencies in Table 2, one can observe that the maximum relative error between the values of the two models is less than 3% for the first eight modes. Furthermore, the mode shapes correlated very well between the original cabin model and the one with the Q-LMFs, as indicated by the high diagonal values of the MAC matrix depicted in Figure 19, except for the 9th and 10th modes.

Setup Validation. The quality of modal analysis relies critically on the quality of the measured FRFs. So before starting the actual data collection, a first set of measurements was performed

Table 2: CAE model without Q-LMFs (Figure 11) vs. CAE model with Q-LMFs (Figure 18).

No.	Without Q-LMFs		With Q-LMFs	
	Freq., Hz	Mode Shape	Freq., Hz	Mode Shape
1	≈ 0	Rigid body	≈ 0	Rigid body
2	44.53	I longitudinal	44.72	I longitudinal
3	85.81	I longitudinal; rigid-body trunk	84.19	I longitudinal; rigid-body trunk
4	112.42	I lateral	109.42	I lateral
5	128.42	II longitudinal; rigid-body trunk	130.10	II longitudinal; rigid-body trunk
6	141.06	I longitudinal; I lateral	140.07	I longitudinal; I lateral
7	150.20	I longitudinal I lateral; I lateral trunk	149.98	I longitudinal; I lateral; I lateral trunk
8	155.57	I vertical	153.53	I vertical
9	178.03	II longitudinal; I lateral I lateral trunk	177.37	
10	181.97		178.80	II longitudinal; I lateral; I lateral trunk
11	201.20	I lateral I vertical I lateral trunk	199.71	I lateral I vertical I lateral trunk
12	205.98	III longitudinal	204.00	III longitudinal

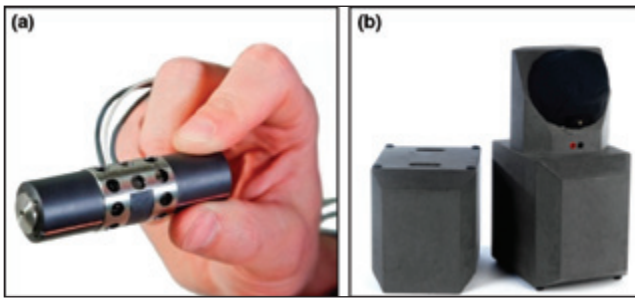


Figure 16. LMS Qsources: (a) Miniature source (Q-IND); (b) Low mid-frequency source (Q-LMF).

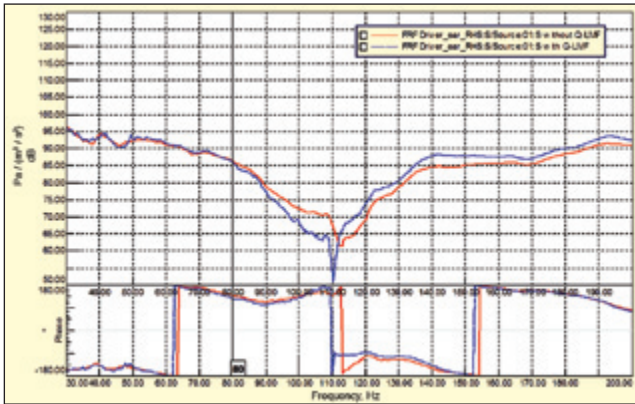


Figure 17. Volume distortion due to presence of Q-LMF source as passive device in car cabin; measured FRF with and without Q-LMF present.

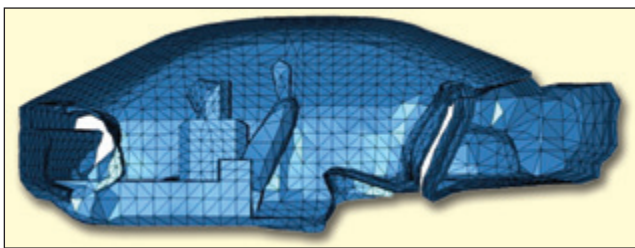


Figure 18. Cabin cross-section and Q-LMF location.

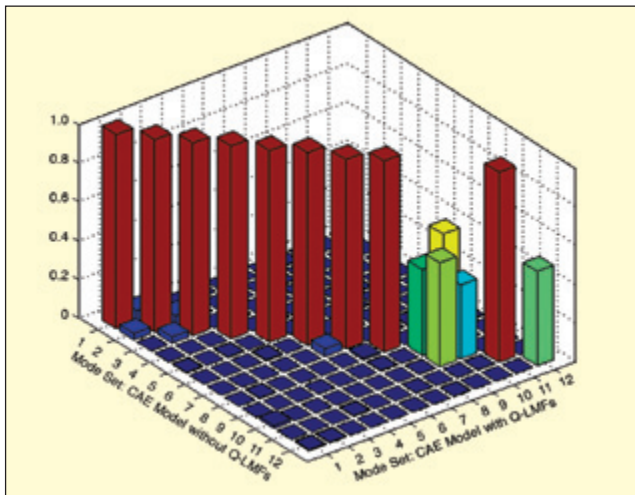


Figure 19. MAC matrix showing mode shape correlation between modes from CAE model without and with Q-LMFs.

to validate data quality features such as: efficiency of inputs, reciprocity, repeatability and linearity. Continuous random white noise was chosen as the excitation signal. The H_1 estimator was used to compute the FRFs based on 150 averages. Typical input auto-power spectra expressed in volume acceleration are shown in Figure 20, where the source signal is very consistent across the different source locations and sources of the same type.

Because of the symmetry, the FRF matrix, which is mathemati-

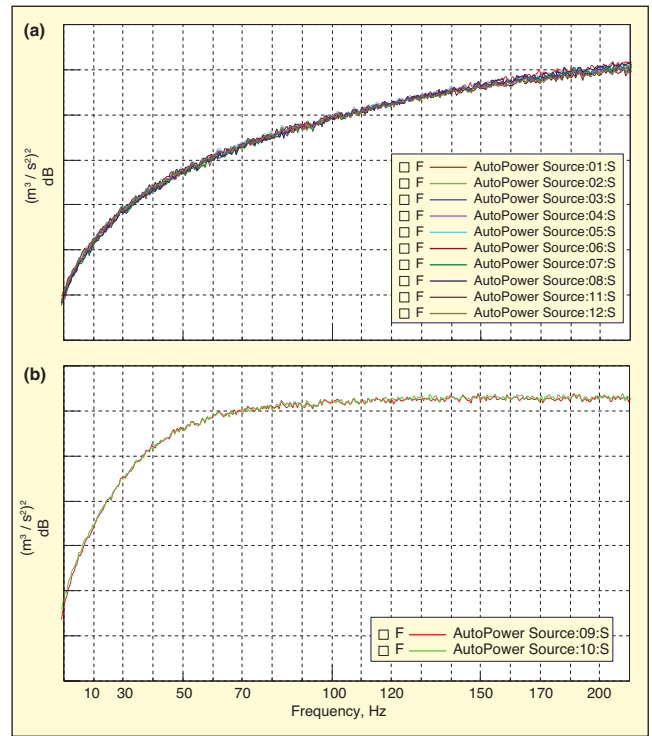


Figure 20. Source auto-spectra with continuous random white noise excitation: (a) Q-IND sources; (b) Q-LMF sources (Y tick divisions = 10 dB).

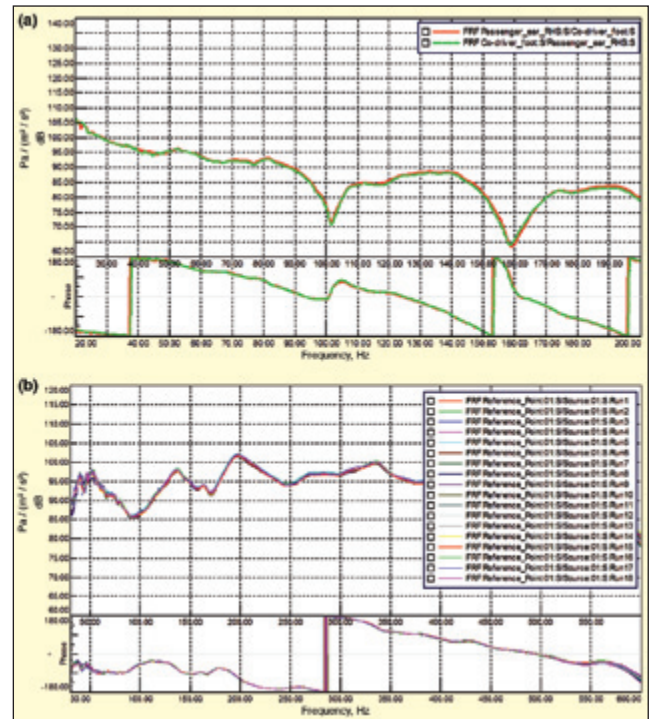


Figure 21. (a) Reciprocity check; (b) Repeatability check.

cally the inverse of the dynamic stiffness matrix, will also be symmetric. So measured FRF data should be identical if the locations of input and output are swapped. Theoretically, this property can be traced back to the symmetry of mass, stiffness and damping matrices. Reciprocity was checked to assess the reliability and accuracy of the measured FRFs. Figure 21a shows an example of a reciprocity check; the amplitude and phase are nearly the same for both reciprocal FRFs over the whole frequency range of interest.

Since during the test procedure, the doors and trunk were opened several times, the repeatability of the measurements was constantly monitored throughout the entire test campaign. This was mainly to ensure that the dynamic behavior of the system and the whole measurement setup system were time invariant.^{15,16} Certain FRFs

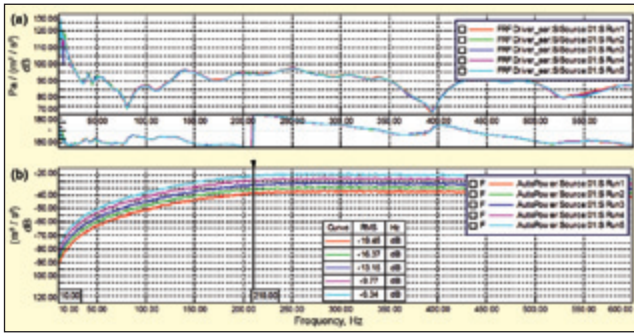


Figure 22. Linearity check: (a) System excited using five different excitation levels; (b) Comparison of FRFs measured at five different excitation levels.

were measured for each run, just to check that neither the system nor the test setup experienced any significant changes. Figure 22b shows the same FRF measured during all 18 runs. It clearly shows that the dynamic behavior of the system was constant and that the testing conditions were kept unaltered throughout the measurement.

As a last check, the linearity of the system was tested by measuring the FRFs at different force levels. If the system is linear, the FRFs will be independent of the excitation amplitudes. Figure 22 shows that the FRFs from the same location measured with different excitation levels are almost identical and confirm the linear behavior of the system.

The validation of the entire measurement chain has proven the high quality of the measurement method being used. The assumption of a time-invariant linear system are guaranteed by checking: the auto-powers of the input; the reciprocal FRFs; the consistency of the data throughout the measurements (repeatability); the system responses for different input levels (linearity); the proper excitation of the system; and the reliability of the inputs.

Experimental Modal Analysis

Preliminary Considerations. An important issue to be addressed when processing acoustic modal analysis data is identifying predominantly acoustic modes in FRFs with a rather high modal density. Even if purely acoustic FRFs have been measured, the modal density is high since the acoustic cabin is coupled to a flexible body and also the resonances of the structural system (mainly panel vibrations from the windshield, the roof, etc.) show up in sound pressure measurements.

So, as already observed in Reference 1, among the several coupled natural frequencies, the number of effective acoustic eigenvalues must be narrowed down to a level that is around the number of uncoupled acoustic eigenvalues computed analytically or numerically. For this purpose, the data acquired by accelerometers placed on strategic positions (windshield, roof, trunk, side windows, etc.) can help to distinguish the dominant acoustic modes: analyzing the structural driving-point FRFs, the main peaks in these FRFs can be considered to be structural modes. If these frequencies are also revealed in the acoustic FRFs, then they can be assumed as not purely acoustic.

Moreover, the high damping of the cabin involves lower and wider peaks in FRFs resulting in highly overlapping modes. Finally, possible data inconsistencies, due to the fact that the different runs were performed in different days, can cause resonance frequencies to vary within the test database. When analyzed altogether, these problems can cause a rather unclear stabilization chart, and hence a non-trivial selection of the right stable pole. Or more precisely, the right stable pole does not exist as such since there are multiple stable poles identifying the same mode.

While the Q-LMF sources are able to excite the low-frequency range quite well, resulting in an excellent coherence from 15 Hz onward (Figure 23a), the Q-IND sources is able to excite the system only from 50 Hz onward. The coherence is indeed rather low up to 30 Hz (Figure 23b). So modal parameters will be extracted in the frequency range from 40 to 200 Hz, excluding the acoustic rigid-body mode (first mode) around 12 Hz.

The mode shape distortion effect discussed earlier can be nicely

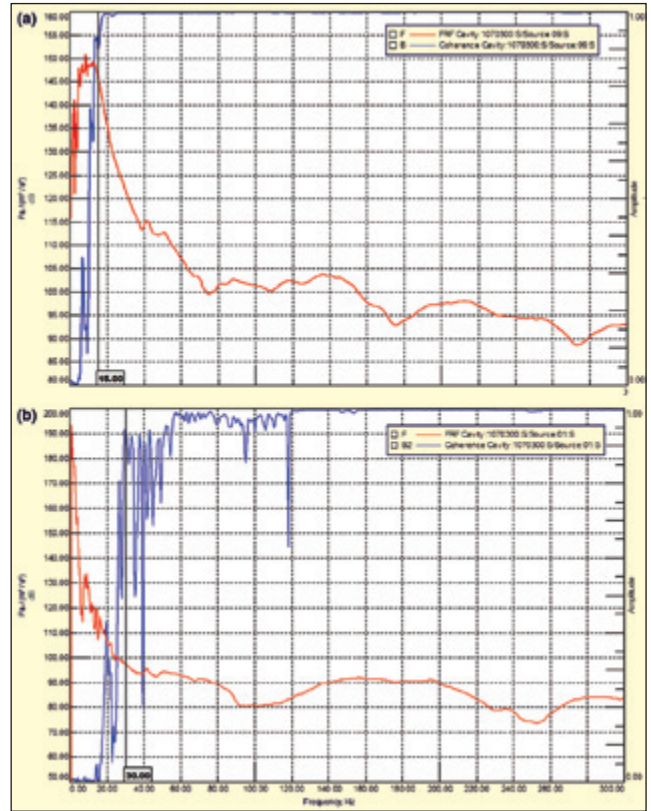


Figure 23. FRF and corresponding coherence: (a) Excitation from low mid frequency source (Q-LMF); (b) Excitation from miniature source (Q-IND).

illustrated using the measurement data. Modal parameters are estimated using all rows of the FRF matrix, but with a different number of columns. Figure 24 compares the use of all 12 columns (12 source locations) with the use of a single column (either the second or third column was selected). While the 12-source case yields a very pure first lateral mode, the shapes of the single-source cases are severely distorted, and the appearance makes it possible to locate the selected source based on the observed mode shape distortions.

As noted previously,^{1,13,17} it was quite challenging for classical modal parameter estimation methods to curve-fit an FRF matrix with so many columns (12 references); typically, not all references are well fitted for a particular sensor location. Also, a very high model order needs to be selected to have a reasonable number of lines in the stabilization diagram (Figure 25), and the diagram itself is a bit less clear. Therefore, a new iterative frequency-domain solver is proposed that has the potential to overcome the difficulties with many references. It is briefly introduced in the next section and afterwards applied to the FRF data.

Maximum Likelihood Estimation Based on the Modal Model.

The so-called ML-MM method^{4,5,17} is a multiple-input, multiple-output (MIMO) frequency-domain estimator providing global estimates of the modal model parameters. In the first step of the ML-MM estimator, initial values of all the modal parameters (poles, mode shapes, participation factors, and upper and lower residuals) have to be specified. In the next step, the error between the modal model equation and the measured data is minimized in a maximum-likelihood sense. Assuming the different measured FRFs to be uncorrelated, the ML-MM cost function to be minimized can be formulated as:

$$\ell^{ML}(\theta) = \sum_{o=1}^{N_o} \sum_{k=1}^{N_f} \frac{|H_{oi}^{ML}(\omega_k, \theta) - H_{oi}(\omega_k)|^2}{\sigma_{H_{oi}}^2(\omega_k)} \quad (7)$$

where N_o is the number of outputs, N_i the number of inputs, N_f the number of frequency lines ω_k the circular frequency, $H_{oi}(\omega_k) \in \mathbb{C}$ the measured FRF, $H_{oi}^{ML}(\omega_k, \theta) \in \mathbb{C}$ the modeled FRF, $\sigma_{H_{oi}}(\omega_k)$ the standard deviation of the measured FRF for output o and input i .

Assuming displacement FRFs, $H^{ML}(\theta, \omega_k) \in \mathbb{C}^{N_o \times N_i}$ can be repre-

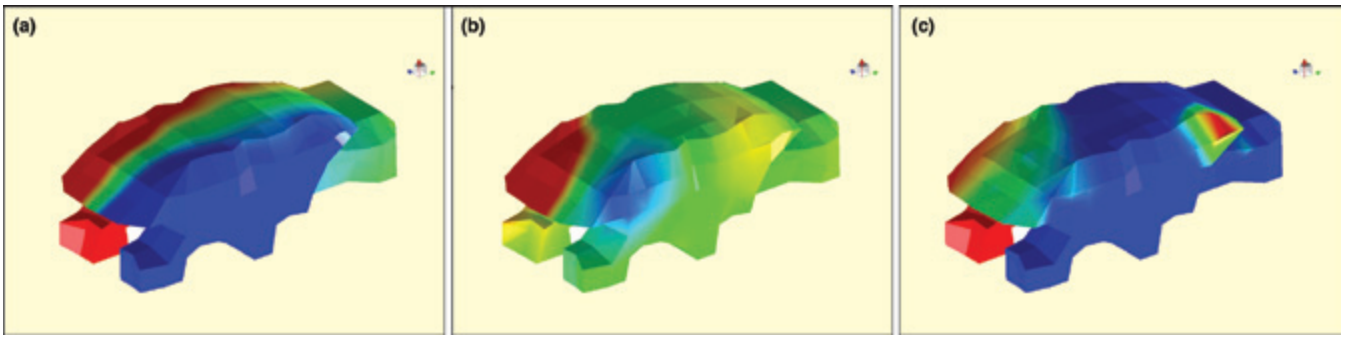


Figure 24. Mode shape distortion of l lateral mode when not using enough acoustic source locations: (a) “Pure” mode shape identified using all 12 sources; (b) Distorted mode shape with one source at Location 2 (front right); (c) Distorted mode shape with one source at Location 3 (rear left).

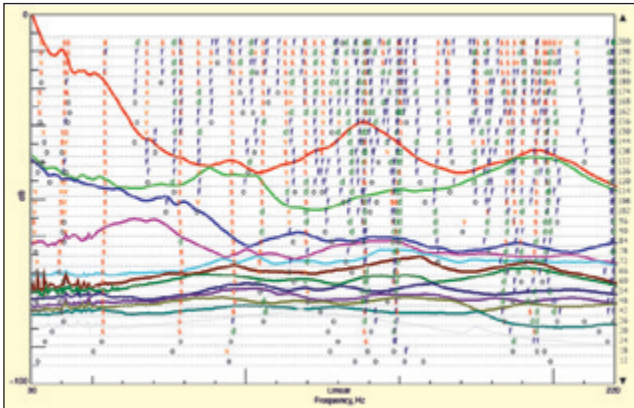


Figure 25. Stabilization diagram obtained by applying Polymax to measured 526×12 acoustic FRF matrix.

sented using the modal model formulation as follows:

$$H^{ML}(\theta, \omega_k) = \sum_{r=1}^{N_m} \left(\frac{\psi_r L_r}{s_k - \lambda_r} + \frac{\psi_r^* L_r^*}{s_k - \lambda_r^*} \right) + \frac{LR}{s_k^2} + UR \quad (8)$$

with N_m the number of identified modes, $\psi_r \in \mathbb{C}^{N_o \times 1}$ the r -th mode shape, λ_r the r -th pole, $S_k = j\omega_k$, $()^*$ stands for the complex conjugate of a complex number, $L_r \in \mathbb{C}^{1 \times N_i}$ the r -th participation factor, $LR \in \mathbb{R}^{N_o \times N_i}$ and $UR \in \mathbb{R}^{N_o \times N_i}$ the lower and upper residual terms. The lower and upper residual terms are modeling the influence of the out-of-band modes in the considered frequency band. The maximum likelihood estimates of θ (i.e., ψ_r , L_r , λ_r , LR , and UR) will be obtained by minimizing the above-mentioned cost function $\ell^{ML}(\theta)$.

This will be done using the Gauss-Newton optimization algorithm. To ensure convergence, the Gauss-Newton optimization is implemented together with the Levenberg-Marquardt approach, which forces the cost function to decrease.¹⁸ To start the optimization algorithm, initial values for all the modal parameters are estimated by the Polymax method.³ More details about the ML-MM method (mathematical implementation, uncertainty derivation, etc.) are presented in References 4,5 and 17.

Results and Comparison. The initial values generated by applying the Polymax method to the full 526×12 FRF matrix (Figure 25) were improved by applying the ML-MM method. The analysis was stopped after 20 iterations, and the convergence is illustrated in Figure 26. Nine pure acoustic modes are well identified in the frequency range from 0-200 Hz (Figure 27). The initial mean fitting error between measured FRFs and Polymax synthesized FRFs was around 9%. The mean fitting error after applying the ML-MM method reduced to only 2%. This improved overall curve fit is illustrated using two typical elements from the full FRF matrix in Figure 28

As visible in Table 3 and Figure 29, the extracted modes are well in line with those already estimated by Polymax. Modes 7 and 8 have been reversed in order during the ML-MM iterations. The MAC between Polymax and ML-MM decreases for increasing mode number. Some differences between Polymax and the ML-MM method can be seen in terms of the frequencies and damping estimates (damping generally increases with reference to the initial Polymax estimates). Actually, these changes in the ML-MM

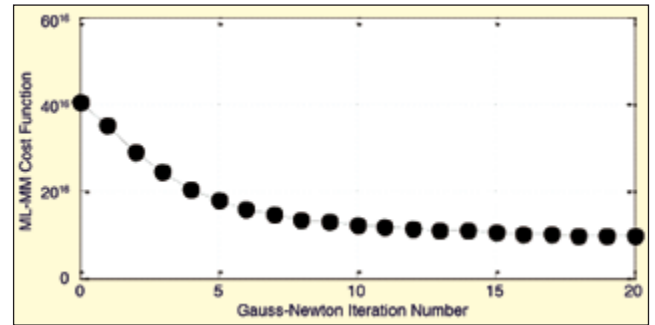


Figure 26. Decrease of ML-MM cost function at each iteration.

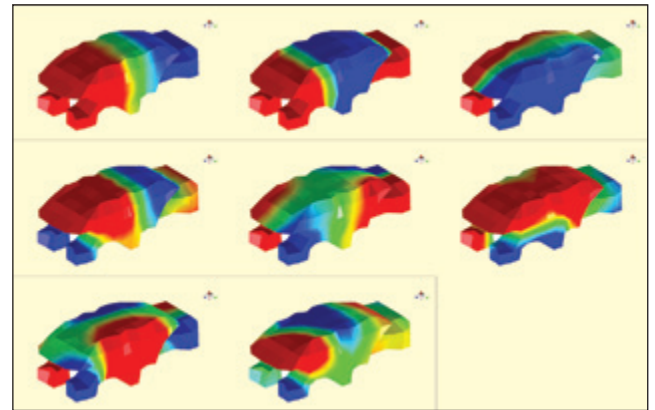


Figure 27. Identified mode shapes using all 12 references; rigid-body mode not shown.

are precisely triggered by the differences between measured and synthesized FRFs. At each iteration, the difference gets smaller.

Conclusions

An intensive test campaign was carried out to characterize the interior acoustic field of an automotive cabin. Equipment and test procedure were detailed and a CAE model of the cabin was used to study the optimal source distribution to place the exciters close to the antinodes. The geometry of the measurement points was also initially defined with the help of the CAE model and afterwards based on the true microphone locations. Such an FE model proved extremely useful both to quantify the influence of the Q-LMF sources on the interior acoustic field and to serve as a baseline on the expected pure acoustic modes. Once the measurement chain was validated, FRFs were measured among 526 microphones on roving arrays and 12 sources switched on sequentially.

Modal parameters were estimated in the frequency range between 40 and 200 Hz by two different methods: Polymax and ML-MM (maximum-likelihood estimation based on a modal model). Nine acoustically dominant modes were identified by both methods and seem to be in line with the numerical ones in terms of mode shapes.

Even for the present case with many references (12), Polymax still yields good modal parameter estimates. These estimates can

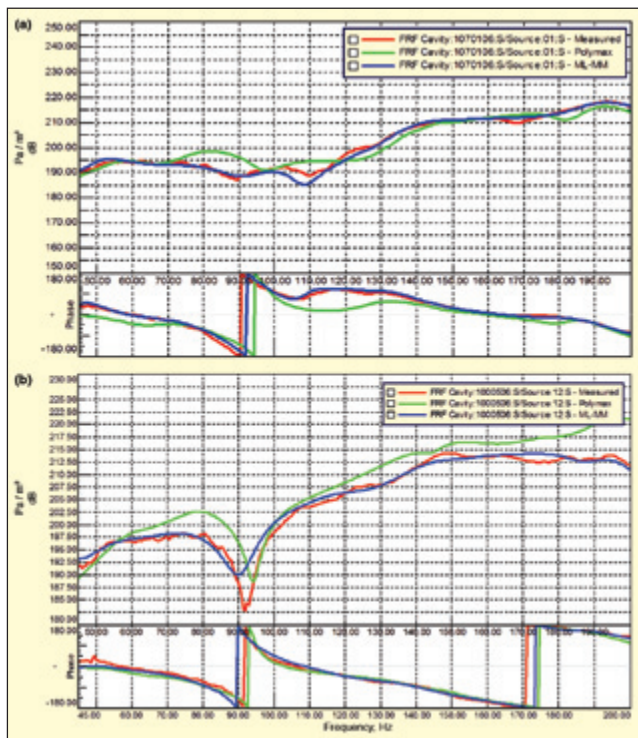


Figure 28. Improved FRF curve-fitting quality shown for two typical FRFs: measured (red), Polymax synthesis (green), ML-MM synthesis (blue).

be further improved by the ML-MM method. These improvements show themselves as improved FRF fitting quality, damping estimation and clarity of the mode shapes. Moreover, the ML-MM method can be implemented as a “one-button function” once the Polymax results are obtained.

We also discussed the new LMS Qsources Low Frequency Monopole Sound Source (Q-MED) that is compact, omnidirectional and capable of generating high noise levels in the low frequency range. A detailed experimental validation study was performed that confirmed that the new source is well suited for automotive cabin acoustic modal analysis.

The article also indicates that care must be taken in selecting the number and location of acoustic sources, since too few source locations will lead to distorted mode shapes.

Acknowledgements

The authors would like to thank the Siemens industry software colleagues Simone Manzato, for his always highly valuable suggestions, and Tom Knechten, for providing valuable information about the LMS Qsources.

We also appreciate the financial support of the European Commission (EC), through its FP7 Marie Curie ITN EID project “ENHANCED” (Grant Agreement No. FP7-606800), and of the

Table 3. Comparison of modal parameters.

No.	Polymax		ML-MM		Mode Shape
	Freq., Hz	Damp., %	No.	Freq., Hz	
2	52.54	12.89	2	51.06	I longitudinal
3	78.12	12.46	3	81.44	I longitudinal; rigid-body trunk
4	96.08	9.22	4	97.24	I lateral
5	138.04	6.31	5	137.79	II longitudinal; rigid-body trunk
6	145.74	11.72	6	148.66	I vertical
7	148.37	9.24	8	150.74	I longitudinal; I lateral; I lateral trunk
8	149.97	4.72	7	149.34	I longitudinal; I lateral
9	194.22	7.82	9	195.13	III longitudinal

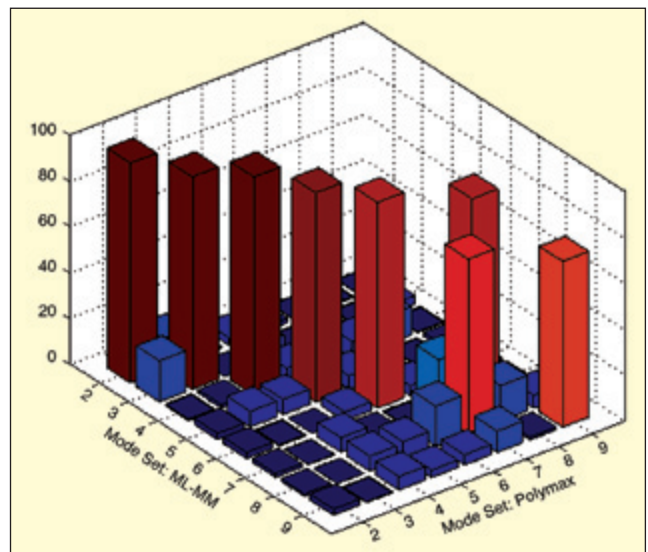


Figure 29. MAC between the initial Polymax mode shapes and final ML-MM mode shapes.

IWT (Flemish Agency for Innovation by science and Technology), through its Innovation mandate IWT project 130872.

References

1. T. Yoshimura, M. Saito, S. Maruyama, S. Iba, “Modal Analysis of Automotive Cabin by Multiple Acoustic Excitation,” Proceedings of ISMA, 2012.
2. H. Tsuji, S. Maruyama, T. Yoshimura, E. Takahashi, “Experimental Method Extracting Dominant Acoustic Mode Shapes for Automotive Interior Acoustic Field Coupled with the Body Structure,” SAE Technical Paper 2013-01-1905, 2013.
3. B. Peeters, H. Van der Auweraer, P. Guillaume, J. Leuridan, “The PolyMAX Frequency-Domain Method: a New Standard For Modal Parameter Estimation,” *Shock and Vibration*, 11: 395-409, 2004.
4. M. El-Kafafy, T. De Troyer, B. Peeters, P. Guillaume, “Fast Maximum-Likelihood Identification of Modal Parameters With Uncertainty Intervals: A Modal Model-Based Formulation,” *Mech. Syst. & Sign. Proc.* 37:422-439, 2013.
5. M. El-Kafafy, P. Guillaume, T. De Troyer, B. Peeters, “A Frequency-Domain Maximum Likelihood Implementation Using The Modal Model Formulation,” Proceedings of SYSID, Brussels, 2012.
6. F. Fahy, P. Gardonio, *Sound Structural Vibration. Radiation, Transmission and Response*, Academic Press, London, 1985.
7. R. Ohayon, C. Soize, “Structural Acoustics and Vibration. Mechanical Models,” *Variational Formulations and Discretizations*, Academic Press, London, 1998.
8. S. Dhandole, S.V. Modak, “A Constrained Optimization Based Method for Acoustic Finite-Element Model Updating of Cavities Using Pressure Response,” *App. Math. Modelling*, 36: 399-413, 2012.
9. W. Heylen, S. Lammens, P. Sas, *Modal Analysis. Theory and Testing*, PMA – K.U. Leuven, 2012.
10. K. Wyckaert, F. Augusztinovicz, P. Sas, “Vibro-Acoustical Modal Analysis: Reciprocity, Model Symmetry, and Model Validity,” *J. Acoust. Soc. Am.* 100 (5):3172-3181, 1996.
11. H. Tsuji, T. Enomoto, S. Maruyama, T. Yoshimura, “A Study of Experimental Acoustic Modal Analysis of Automotive Interior Acoustic Field Coupled with the Body Structure,” SAE Technical Paper 2012-01-1187, 2012.
12. K. Wyckaert, L. Meulewaeter, “On the Influence of Finite Acoustic Source Dimensions on Acoustical Frequency Response Functions inside an Enclosed Cavity,” Proceedings of ISMA, 1996.
13. B. Peeters, M. El-kafafy, G. Accardo, T. Knechten, K. Janssens, J. Lau, L. Gielen, “Automotive Cabin Characterization by Acoustic Modal Analysis,” Proceedings of JSAE Spring Annual Conference, 114-20145437, 2014.
14. C. Coster, D. Nagahata, P.J.G. van der Linden, “On the Accuracy Reciprocal and Direct Vibro-Acoustic Transfer-Function Measurements on Vehicles for Lower and Medium Frequencies,” Proceedings of ISMA, 2010.
15. J. He and Z.F. Fu, *Modal Analysis*, Butterworth-Heinemann, Oxford, 2001.
16. D. J. Ewins, *Modal Testing: Theory, Practice and Application*, Research Studies Press Ltd., 2000.
17. M. El-kafafy, G. Accardo, B. Peeters, K. Janssens, T. De Troyer, P. Guillaume, “A Fast Maximum Likelihood-Based Estimation of a Modal Model,” Proceedings of the 33rd International Modal Analysis Conference, Orlando, 2015.
18. P. Eykhoff, *System Identification: Parameter and State Estimation*, John Wiley & Sons Ltd., Bristol, 1979.

The author can be reached at: bart.peeters@siemens.com.